IEEE Open Journal of
Vehicular Technology

Received 24 January 2022; accepted 15 February 2022. Date of publication 22 February 2022;
date of current version 31 March 2022. The review of this article was coordinated by Editor Edward Kwok Shum Au.

Digital Object Identifier 10.1109/OJVT.2022.3152699

Self-Organizing Multilateration of an Unknown Number of Transmitters

KYLE W. MCCLINTICK (Student Member, IEEE), JEFFREY TOLBERT (Student Member, IEEE), AND ALEXANDER M. WYGLINSKI (Senior Member, IEEE)

Wireless Innovation Laboratory, Worcester Polytechnic Institute, Worcester, MA 01609 USA

CORRESPONDING AUTHOR: KYLE WILLIAM McCLINTICK (e-mail: kwmcclintick@wpi.edu)

ABSTRACT Wireless Sensor Networks (WSNs) that classify the source of detected radio signals require mobile transmitters, physical (PHY) and link layer meta data, and packet sniffing capabilities. These signal classifiers are restricted by assumptions that may be difficult to realize in adversarial Signal of Opportunity (SOP) localization settings, and they do not jointly localize transmitters. In this paper, we present a novel framework that self-organizes to classify and jointly localize sets of stationary transmitters emitting SOP. The framework leverages the underlying Gaussian distribution associated with multilateration estimates via the use of Unsupervised Learning (UL) techniques. Inference of spatial multilateration features allows for the joint estimation of classification outcomes with respect to several unknown parameters, including the number of transmitters, source transmitters for each signal, the underlying multilateration distribution, and the transmitter locations. The proposed framework was evaluated in a two-dimensional trilateration experiment. Signals transmitted by vehicular Tire Pressure Monitoring System (TPMS) wireless beacons were observed by a custom-built WSN test bed to produce Received Signal Strength Indicators (RSS) features. We used a trained Convolutional Neural Network (CNN) to make location estimates from the RSS feature data. An Anderson-Darling test showed that these CNN estimates were statistically indistinguishable from those of a normal distribution. The spatial trilateration estimates were clustered to identify six of the eight TPMS transmitters with a 75% cluster detection rate, which was the result of every statistically different spatial and RSS population as determined by a Kruskal-Wallis (KW) test. The source transmitter of every signal was classified with a 76.4% indicator variable accuracy (93.7% when removing statistically identical RSS populations) and the detected source transmitters were localized with an average of 1.72 m variance and 1.19 m bias within a roughly 15 m square whose perimeter is made up of receivers.

INDEX TERMS Convolutional neural network, dirichlet process Gaussian mixture model, fingerprinting, multilateration, signals of opportunity, unsupervised learning, wireless localization.

NOMENCLATURE

ACRONYMS

AD	Anderson-Darling
ADS-B	Automatic Dependent Surveillance Broadcast
AUC	Area Under the Curve
CDF	Cumulative Distribution Function
CDMA	Code Division Multiple Access
CFAR	Constant False Alarm Rate
CNN	Convolutional Neural Network
CRLB	Cramer Rao Lower Bound
DPGMM	Dirichlet Process Gaussian Mixture Model
DTV	Digital Television
EM	Expectation Maximization
GNSS	Global Navigation Satellite System
GPS	Global Positioning System
GSM	Global System for Mobile Communications
KW	Kruskal-Wallis
LIDAR	Light Detection and Ranging
LOS	Line of Sight
MCMC	Markov Chain Monte Carlo
MHT	Multi-Hypothesis Tracking
MSE	Mean Squared Error

NLOS	Non Line of Sight
NN	Neural Network
OOK	On-Off Keying
PLL	Phase-Locked-Loop
PPV	Positive Predictive Value
QQ	Quantile-Quantile
ReLU	Rectified Linear Unit
RF	Radio Frequency
ROC	Receiver Operating Characteristic
RSS	Received Signal Strength
SGD	Stochastic Gradient Descent
SL	Supervised Learning
SOI	Silicon on Insulator
SOP	Signal of Opportunity
TDoA	Time Difference of Arrival
TPMS	Tire Pressure Monitoring System
UL	Unsupervised Learning
UWB	Ultra Wide-Band
VI	Variational Inference

I. INTRODUCTION

Driverless vehicles could save the U.S. economy an estimated $450 billion per year [1] by improving traffic safety [2], [3], increasing the mobility of the impaired and the elderly [4], and reducing pollution to the environment [5]. To realize robust autonomous operation, vehicles require nearly comprehensive and continuous situational awareness to make appropriate driving decisions. This awareness is obtained via the use of on-board sensing technologies such as LIDAR (LIDAR) [6], computer vision algorithms [7], [8], and radar [9]. A GNSS (GNSS) such as GPS (GPS) or similar provides vehicle location data. [10]. Accurate location information is critical, especially during maneuvers such as lane changing, navigating an intersection, or merging with high speed traffic [11]. GNSS-based techniques may be unable to handle complex road conditions upon which these vehicles operate, such as urban canyons [12] and foliage [13] that cause significant signal attenuation, as well as being susceptible to unintentional interference [14] and malicious jamming signals [15]. Therefore methods to supplement or replace GNSS have generated significant interest [16].

Alternatively, the position and velocity of vehicles can also be determined by leveraging SOP (SOP)-based navigation and beacon localization methods, which assume that source transmitters detected by the WSN can be distinguished using a priori metadata (*e.g.*, physical layer attributes such as carrier frequency). However, in adversarial wireless localization problems, this meta data may be limited or unavailable. In this work, we introduce a framework to estimate and classify the following unknown parameters using only physical pass-band signal characteristics detected by the WSN: *i*) the number of transmitters; *ii*) their location; *iii*) which transmitter sent each detected signal. State-of-the-art WSN frameworks that estimate a subset of or all of these unknowns include ADS-B (ADS-B) signals used in aerospace applications [17]–[22]. These solutions estimate RF (RF) features that are highly correlated to hardware noise such that the transmitters can be identified [17], [18], perform mobility analysis via Multi-Hypothesis Tracking (MHT) [19], use heuristic thresholds in multilateration or range estimate based verification methods [20], [21], or employ a combination of these techniques [22].

Although there have been substantial advances in SOP-based localization and navigation, several challenges remain. Radio-frequency (RF) feature analysis solutions such as the algorithms presented by Moser *et al.* [17] and Schafer [18] require protocol meta data, including transmission frequency, to correct for Doppler effects when computing their frequency-based feature. Additionally, Moser's phase-based feature requires the detection of spoofing signals transmitted during the tuning interval of the spoofer's Phase-Locked-Loop (PLL), during which the transmitter-specific transient behaviors can be observed. Mobility analysis works such as [19] reliably detect sudden changes to tracks, but can be vulnerable to slowly diverging spoofed tracks and spoofers who are knowledgeable of the propagation delay to trusted transmitters. Multilateration and range-estimate based verification methods also have several drawbacks, including heuristic-based thresholding techniques for classification that do not generalize well, along with requirements for non-opportunistic signals to contain position and time stamp information. Moreover, they employ inference techniques that focus only on the binary unknown parameter representing the presence or absence of a second transmitter or spoofer.

In this paper, we present a novel algorithmic framework distinguished from other state-of-the-art for low assumption multilateration networks in the following ways:

1) The framework provides a stationary alternative to MHT that is relatively computationally inexpensive by utilizing Bayesian clustering instead of hypothesis test trees.
2) It introduces an opportunistic alternative to current WSNs that use multilateration data to classify signal source IDs, allowing for localization without packet sniffing.
3) The framework requires fewer assumptions compared to current RF signature-based WSNs that use phase and frequency meta data, allowing for the localization of transmitters when little is known *a priori* by the WSN about RF behavior.

The rest of this paper is organized as follows. Section II presents a detailed overview of the SOP concept, the value of meta data, and the goals of our approach. Section III describes the framework as well as details of our methodology and experimentation. Section IV evaluates the performance of our CNN-based multilateration and UL-based clustering of spatial multilateration data. This analysis includes an Anderson Darling (AD) normality test of spatial data to confirm the Gaussian assumptions of the UL algorithm, as well as a

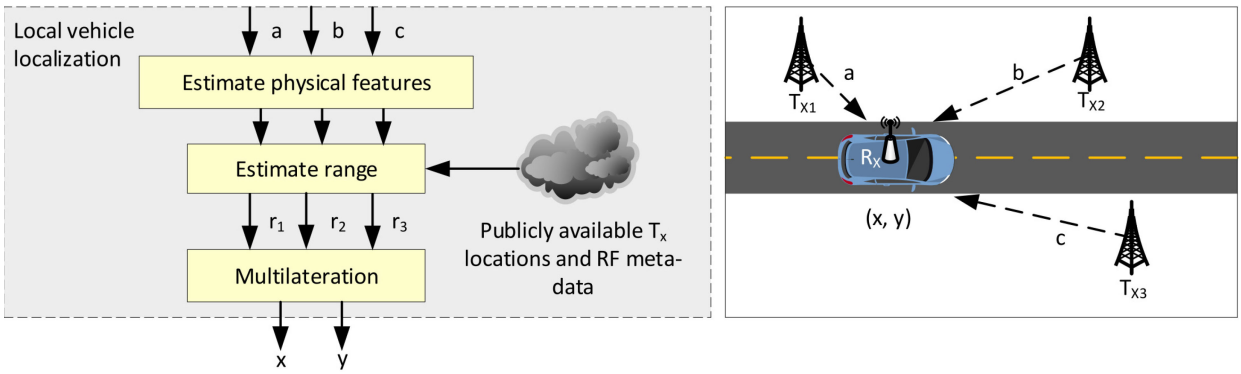

(a) Outdoor receiver localization

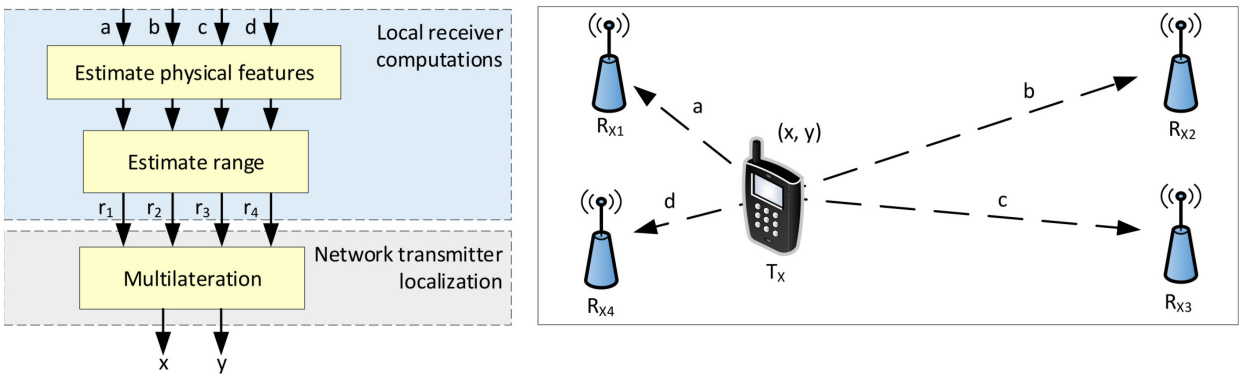

(b) Indoor transmitter localization

FIGURE 1. **Complementary SOP navigation scenarios: (a) Vehicle determines its location based on ranging of source transmitters; (b) transmitter location determined based on its emissions detected passively by network of WSN receivers. Physical feature and range estimates are independent of other readings in the SOP beacon localization problem, such that they may be computed locally at each receiving sensor or at the fusion center.**

Kruskal-Wallis (KW) non-parametric test of Received Signal Strength (RSS) estimates. Final thoughts are discussed in Section V, including drawbacks and open challenges of our methodology.

II. OVERVIEW OF LOCALIZATION MODEL

A SOP is a wireless signal that is both freely available but not designed to carry information for receiving localization systems [23]. SOP-based navigation systems perform multilateration given a user's receiver with an unknown location. Several local transmitters with known locations are used with enough wireless information known about their carrier frequency and bandwidth to individually detect each signal and estimate physical properties from them. These systems (Fig. 1 (a) typically use high altitude, high transmit power SOPs such as DTV (DTV), GSM (GSM), and CDMA (CDMA) signals in outdoor multilateration experiments with a small number of SOP transmitters [24]–[26]. System performance for these approaches varies greatly depending on the availability and orientation of the transmitters, and their advantages and disadvantages have been sufficiently covered in [16], [23].

SOP-based navigation researchers have also explored the inverse approach focusing on the beacon localization problem. In this approach, several receivers with known locations are used together to estimate the positions of one or more SOP-emitting transmitters with unknown locations (Fig. 1 (b). They usually report SL (SL)-based, RSS-based indoor multilateration [27] or parameterized fingerprinting experiments to estimate the location of a single Zigbee, Wi-Fi, Bluetooth, or UWB (UWB) SOP transmitter via multiple receivers [28]–[33]. System performance for these works varies greatly depending on the SL algorithm used, training data collected, and the number, placement, and design of the receivers.

In this work, we investigated a variant of the transmitter localization scenario, where a WSN "black box" had to solve the problem without meta data or packet sniffing capabilities (Fig. 2). Metaphorically speaking, the "black box" represents the WSN operator's intent to localize any detectable signals. Without *a priori* knowledge of how the channel activity corresponds to transmitter activity or packet-layer data such as reported transmitter location [17]–[22], our WSN was forced to use only locally-computed physical signal characteristics (*e.g.*, Time Difference of Arrival (TDoA), RSS) to determine the source of each detected signal while also locating and counting those source radios. Given that pre-multilateration

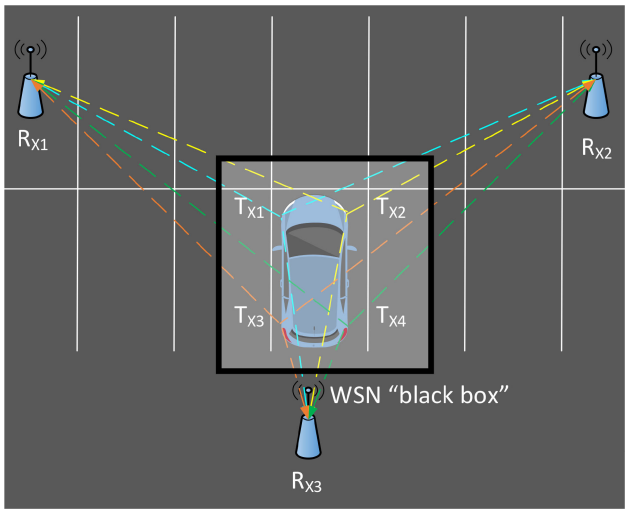

FIGURE. 2. An example of the low meta data scenario is a subset of the transmitter localization problem, where the number of beacons is hidden from the localization network of sensors, and must be inferred. As in the standard localization problem, the transmitter locations are unknown. Additionally, the origin of the four signals detected in this scenario is hidden, such that the receiving network must infer which transmitter sent which signal via the physical layer pass-band characteristic inference of signal strength, angle, or timing estimates.

physical features in this complex WSN varied by protocol, time, frequency, bandwidth, and several other physical characteristics, a post-multilateration clustering approach was needed to leverage the sum-of-Gaussians characteristic of all CNN multilateration estimates despite their front-end variations.

III. PROPOSED MULTILATERATION FRAMEWORK

In this section, we describe our framework (see Fig. 3). The method begins with the signal detection and pre-processing of the TPMS signals received by our WSN setup, their processing by a central computer to produce several input features, generation of spatial transmitter location estimates from those features via CNN-based multilateration, and UL-based inference of unknown parameters leveraging that spatial data.

A. SIGNAL DETECTION AND PRE-PROCESSING

Data files in the form of two-dimensional arrays were processed to generate RSS estimates from each receiver for each TPMS frame over time before localization could occur (block (a) in Fig. 3). The process of extracting RSS estimates from a given data file includes: down-sampling, frame detection, preamble frequency and timing correction, and frame correlation for estimating the RSS per frame.

The first step required band-pass filtering and down-sampling to reduce the computational load as well as increase the effective bit depth resulting from oversampling.

After re-sampling, detection was performed. This step began by identifying the start of each individual frame. For this application we used a simple power detector with a Constant

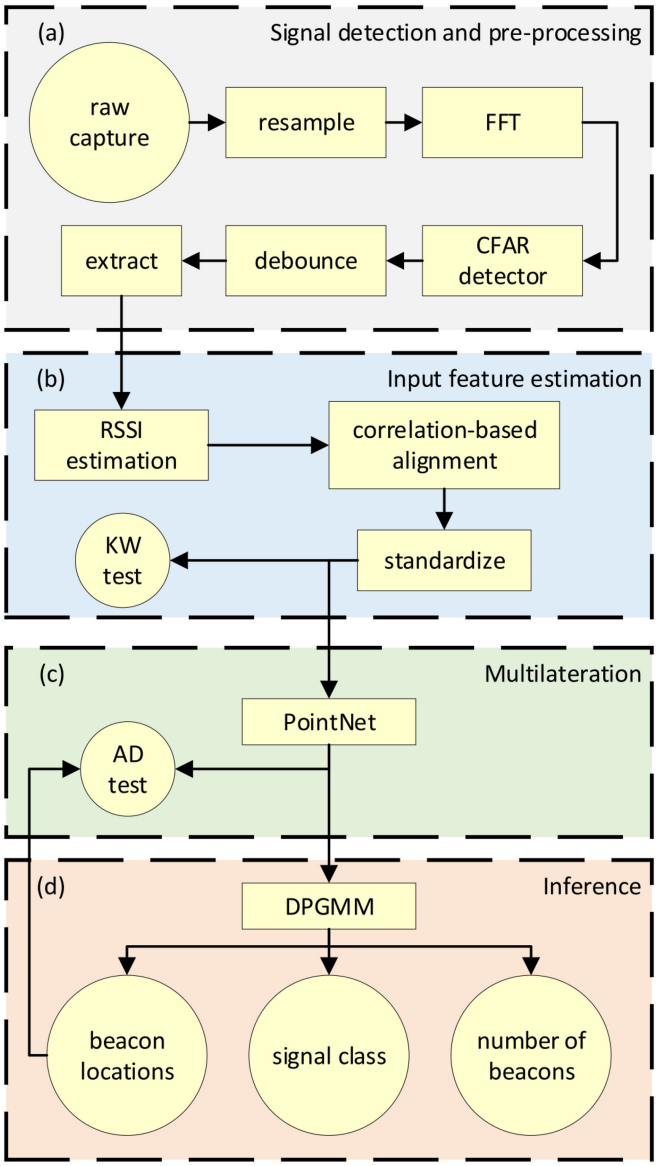

FIGURE 3. An overview of the interaction between of all estimators, classifiers, and digital signal processing tasks of the proposed approach presented in this work. Inputs and outputs are represented by circles, while intermediate steps are represented by rectangles. KW and AD tests were performed to determine the uniqueness of each beacon's true RSS population and normality of estimated beacon location subtracted multilateration estimates, respectively. Normality is an assumption of the DPGMM (DPGMM) inference, and by determining the number of unique input data populations, we identify maximum performance bounds for the DPGMM inference.

False Alarm Rate (CFAR) threshold. We started by decomposing the down-sampled file into $k = 1, \ldots, K$ bins based on the detector's integration period T. The energy level of each bin in the decomposed signal $x(t)$ was computed as [34]:

$$E[k] = \frac{1}{T} \int_{Tk}^{T(k-1)} \|x(t)\|^2 dt. \quad (1)$$

For this type of CFAR detector, the threshold level is computed using [35]:

$$\alpha = N(P_{\text{fa}}^{-1/N} - 1), \tag{2}$$

given false alarm probability P_{fa} and number of samples N.

B. INPUT FEATURE ESTIMATION

After a frame was detected, the frequency and timing errors had to be corrected before the RSS can be estimated using correlation (see block (b) in Fig. 3). The frequency and timing offsets form a continuous ambiguity function (CAF). To estimate the frequency and timing offset parameters, the known preamble was frequency shifted and stretched as needed, then correlated against the detected frame. The peak of the correlations represented the best fit. This technique allowed for varying degrees of accuracy but at the expense of computational load. For this experiment, we post-processed the data on a desktop such that computational resources were not a limiting factor. The correlation between the CAF search preamble and the received signal also acted to estimate the RSS of the received frame [36]:

$$\text{RSS} = \frac{1}{N}\sum_{t=1}^{N} x_t ||\hat{x}_t||, \tag{3}$$

where x_t sampled from $t = 1, \ldots, N$ is the CFAR detected signal and $\hat{x}_t$ is the unit power CAF preamble after correcting for frequency and timing offsets. Through this process, we employed three receivers to produce a dataset where input features were represented as $x = [\text{RSS}_1, \text{RSS}_2, \text{RSS}_3]$.

Algorithm 1: CNN model training protocol [40].

procedure Given training data X, labels Y, learning rate η, training iterations n_e
  initialize model parameters w, b
  for n_e **do**
    for each x in X, y in Y **do**
      for layer convolution layer l in L **do**
        for filter w in layer l **do**
apply zero-padding if used
compute convolution $z_l(x, w, b)$
apply ReLU $a = \max(0, z)$
compute max pooling $P = \text{pool}(a)$
        end for
      end for
      flatten down sampled features, $p = \text{flatten}(P)$
      for each dense layer **do**
        compute linear logit, $z(p, w, b)$
        compute activation function $a = \max(0, z)$
      end for
      compute softmax $\hat{y} = \arg\max(a(z))$
      compute loss $f_{CE}(y, \hat{y})$
      compute gradients $\frac{\delta}{\delta w} f_{CE}$, $\frac{\delta}{\delta b} f_{CE}$
      update model parameters w, b
    end for
  end for
end procedure

C. MULTILATERATION

Multilateration (see block (c) of Fig. 3) is the process of using physical signal characteristics to estimate the distance between receiver-transmitter pairs, and subsequently computing the transmitter's most likely location. The CNN algorithm is a popular choice for replacing both stages of multilateration with a set of trainable weights [28]–[33]. This algorithmic substitution is useful for replacing fingerprinting methods because it allows for continuous, rather than discrete-space, unknown parameter estimation through the use of trainable weights. This attribute is important since physical space is a continuous variable, and traditional fingerprinting typically predicts physical transmitter location via nearest-neighbor techniques that introduce inherent errors due to their discrete-space nature [28]–[33]. Alternatively, traditional continuous-space, physical characteristic-based transmitter localization techniques first estimate the range by assuming an electromagnetic signal propagation path loss model, then solve for the geometric problem of intersecting circles (or parabolas) to identify the most likely region of the transmitter [37]. State-of-the-art CNN localization works [28]–[33] use the universal approximator characteristic [38] of Neural Networks (NNs) to provide flexible, accurate transmitter location estimates that improve traditional fingerprinting and provide an alternative to multilateration if the training data is available. Although range and geometry solving multilateration methods do not require training data, they do require meta data in the form of path loss information [39].

Although CNN architectures can take many forms, the SGD (SGD) training methodology is frequently employed (see Algorithm 1) [40]. A NN can be described as a union of small non-linear regression models arranged in both parallel and serial connections. In our case, these models were iteratively optimized via SGD to minimize the estimation error of each transmitter's location. The use of filters in the CNN architecture can be described as enforcing a constraint on weights that results in model regularization, lower computational costs, and the model assumption of input equivariance. Input equivariance is the idea that data patterns correlated to the ground truth are highly similar despite shifts, rotations, and other common transforms.

D. INFERENCE

Using clustering algorithms as the final step in our proposed methodology, we proceeded to estimate or classify the unknown parameters described in Section I (see block (d) in Fig. 3). This was achieved by self-organizing the spatial transmitter location estimates provided by the CNN. Membership in a cluster represents the probability the signal that produced that location estimate was transmitted by the same radio as all

other location estimates in that cluster. The number of active clusters represents the probability of how many radios transmitted the set of all signals detected by the WSN. Finally, the estimated mean of each cluster represents the most probable location of a transmitter.

The DPGMM assumes a set of samples was generated by the following generative conditional distribution [41]:

$$p(P_i|\pi_1, \ldots, \pi_k, \mu_1, \ldots, \mu_k, s_1, \ldots, s_k) = \sum_{j=1}^{k} \pi_j \mathcal{N}(\mu_j, s_j^{-1}), \quad (4)$$

where the mixing proportions $\sum_{j=1}^{k} \pi_j = 1$, and observations from Gaussians of mean μ and covariance s^{-1} with larger mixing proportions π are generated more often, and mixing proportions that are small indicate inactive mixtures. Since integrating to evaluate the distributions $p(\pi_1, \ldots, \pi_k|P_1, \ldots, P_N) \propto p(P_1, \ldots, P_N|\pi_1, \ldots, \pi_N)p(\pi_1, \ldots, \pi_N)$ are not tractable, Bayesian inference of DPGMMs is always performed either by MCMC (MCMC) sampling [42], VI (VI) [43], or EM (EM) [41]. In this work, we employed the optimization-based EM as a relatively hands-off approach when compared to VI or MCMC, which only risks convergence to a local minima [44]. MCMC and VI, on the other hand, risk mode default and poor mixing due to their utilization of Gibbs sampling [44]. Additionally, EM provides faster and more accurate results for when point estimates are sufficient, as in this study [44].

EM optimization of the DPGMM conditional probabilities $\theta = \pi_1, \ldots, \pi_k, \mu_1, \ldots, \mu_k, s_1, \ldots, s_k$ is then provided first by the expectation step, which computes the cluster indicator vector c of each sample given current estimated distribution parameters [41]:

$$p(c_i = z|P_i, \theta) = \frac{\mathcal{N}(\mu_z, s_z^{-1})\pi_z}{\sum_{j=1}^{k} \mathcal{N}(\mu_j, s_j^{-1})\pi_j}, \quad (5)$$

where observation P_i belongs to mixture z if $p(c_i = z|P_i, \theta) > p(c_i \neq z|P_i, \theta)$.

Then, inversely, the maximization step is given as the computation of the new Bayesian posterior distributions by using the current cluster assignments as:

$$\pi_j = \frac{1}{N} \sum_{i=1}^{N} p(c_i = j|P_i, \theta), \quad (6)$$

$$\mu_j = \frac{\sum_{i=1}^{N} p(c_i = j|P_i, \theta)P_i}{\sum_{i=1}^{N} p(c_i = j|P_i, \theta)}, \quad (7)$$

$$s_j = \frac{\sum_{i=1}^{N} p(c_i = j|P_i, \theta)}{\sum_{i=1}^{N} (P_i - \mu_j)^2 p(c_i = j|P_i, \theta)}. \quad (8)$$

Algorithm 2: Dirichlet Process Gaussian Mixture Model (DPGMM) inference by EM [41].

procedure Given observations P, mixing proportions π, cluster means μ, cluster covariance s^{-1}, indicator variables c, number of observations N and number of clusters k
  Initialize $\theta = \pi_1, \ldots, \pi_k, \mu_1, \ldots, \mu_k, s_1, \ldots, s_k$
  while not converged **do**
    Expectation step
    for $i \in \{1, \ldots, N\}$ **do**
      for $j \in \{1, \ldots, k\}$ **do**
        compute $p(c_i = j|P_i, \theta)$
      end for
    end for
    Maximization step
    for $j \in \{1, \ldots, k\}$ **do**
      for $i \in \{1, \ldots, N\}$ **do**
        compute $\pi_j|p(c_i = j|P_i, \theta)$
        compute $\mu_j|P_i, p(c_i = j|P_i, \theta)$
        compute $s_j|P_i, \mu_j, p(c_i = j|P_i, \theta)$
      end for
    end for
  end while
end procedure

Algorithm 2 shows an overview of the DPGMM EM optimization, including the combination of the expectation and maximization steps.

Current wireless localization works that make use of unsupervised learning algorithms [45]–[48] do so for self-supervised applications, wherein clustering is used to generate labels for unlabeled data such that the costs of training a supervised learning model are reduced. These methods have been shown to reduce the bias and variance of CNN-based fingerprinting estimates.

In previous work, we applied a Gaussian Mixture Model (GMM) to a known number of mobile, simulated wireless beacons [49]. In the following sections, we describe how we applied a modified version of that proof of concept simulation to a practical experiment. There were several differences between the two efforts.

- Mutliateration estimates were produced from real measurements, rather than generated directly from a Gaussian distribution.
- While the Markov process used generated Gaussian samples at each time step with a stationary mean, real-life data sets have a non-stationary mean. This would make the use of mixture models inappropriate, which assume the distributions are stationary.
- We used a Dirichlet prior, which allowed for the inference of an unknown number of clusters instead of a fixed number specified by the user utilizing *a priori* meta data.

FIGURE 4. The experiment site, located at 358 Pleasant St, Gardner MA, USA (longitude -71°59'41.32"W, latitude -42°34'9.19"N). The hardware used in the experiment is also pictured.

Next, we present the implementation details of our novel framework (see Fig. 3), as well as evaluate its performance.

IV. EXPERIMENTAL RESULTS

In this section, we describe the implementation details of the proposed CNN-based multilateration, including the method used to generate dataset ground truths, the architecture used, and the training protocol. We subsequently evaluate our entire methodology (Fig. 3), supplemented by the use of assumption-checking hypothesis testing.

A. EXPERIMENT IMPLEMENTATION DETAILS

Three custom-built Raspberry Pi 3 Model B+ receivers employing NooElec NESDR smart v4 RTL SDR units and isotropic antennas were used to digitize and store the RF signals at 315 MHz emanating from the TPMS sensors of a Subaru Forester 2016 (Fig. 4). For each TPMS sensor, a three minute RF capture was made per location at 2.5 MSPS complex IQ. The experiment consisted of four TPMS sensors, three custom receivers, nine training vehicle positions, and two vehicle positions used for evaluation, which resulted in 132 data files. The samples were loaded into MATLAB and the built-in resample function was used with a re-sampling factor of 32. This resulted in an output bandwidth of 78.125 kHz which was above the silicon on insulator (SOI) bandwidth and was about 18 samples per symbol for the TPMS SOI. Finally, a time constant of $T = 5$ milliseconds was used in our CFAR detector, which used both training cells and guard cells, but only on one side of the cell under test. We used three guard cells and 10 training cells.

B. LABEL GENERATION VIA SURVEYING

To generate the ground truth labels for the training and testing of our CNN, we surveyed the parking lot located at 358 Pleasant St, Massachusetts, USA (longitude -71^{o}59'41.32"W, latitude -42^{o}34'9.19"N). String was used to draw circles with tied sticks of chalk, anchored down to the center of the circles on each of our three Raspberry Pi units, which were used as the sensing localization network (Fig. 5). Since each chalk intersection location was known, the grid allowed physical objects to be located in the experimental region by trilateration via hand-measuring three distances to the three nearest chalk intersects (not to be confused with the wireless multilateration performed by our experiment). Measuring distances to more than three reference points would have increased the accuracy

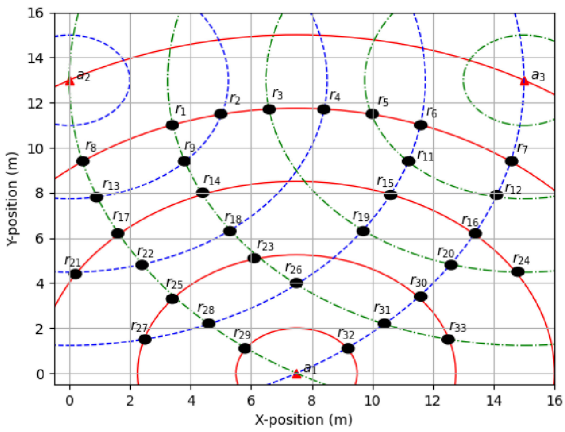

(a) Surveyed reference locations

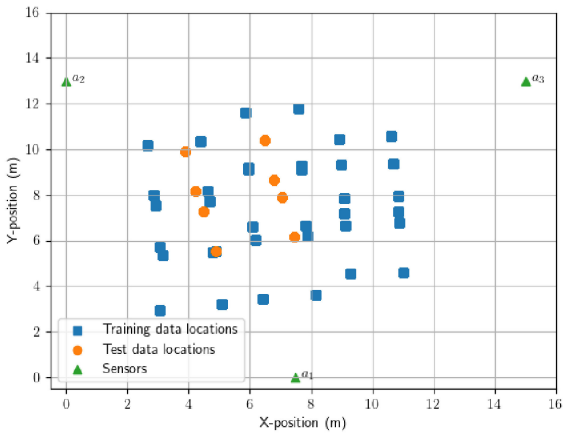

(b) Anchor and beacon placements

FIGURE 5. The true location of beacons was measured by adding the measured distance of the beacon from these known intersect points (a) and the anchor and beacon locations for the experiment (b).

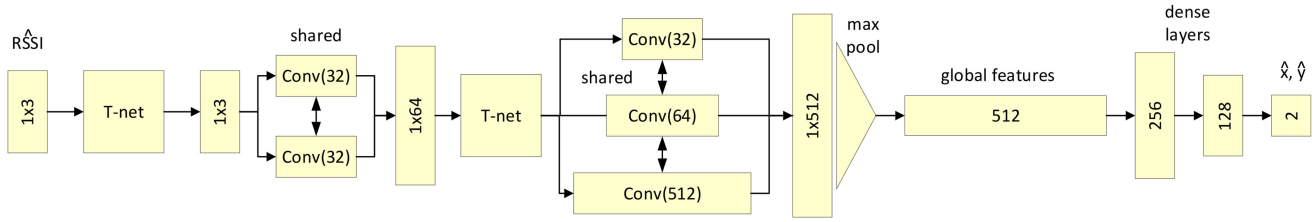

FIGURE 6. An overview of the PointNet CNN architecture, which we modify only by changing the 10-class softmax output to a two-dimensional linear output. A dropout with $p = 0.3$ is used after each dense layer. Each T-net is a mini-network that aims to learn a affine transformation matrix. PointNets are designed for low-dimensional data and physical space. We employed a bagging ensemble of three PointNets for this experiment.

of label generation at the cost of more time spent measuring at each point. The error for the hand-made range measurements of the 32 grid locations given by Fig. 5 was found, in an experiment of 32 measurements, to have a mean error of 2.00 cm and an error standard deviation of 1.68 cm. These moments were determined by comparing theoretical geometry (see Fig. 5) to the actual measurements. This error combines human tape-measure error, which is about 0.5 cm or half a tick mark, and chalk circle intersect misplacement errors caused by slack in the string and its measurement error. Given this statistical description of range measurements, we used the second order Taylor series approximation of the CRLB (CRLB) for multilateration measurements m [50]:

$$\underline{CRLB}(\underline{\theta}|\underline{m}) \geq \left[\frac{d\underline{m}(\underline{\theta})}{d\underline{\theta}}^T \underline{N}(\underline{\theta})^{-1} \frac{d\underline{m}(\underline{\theta})}{d\underline{\theta}} + \frac{1}{2} tr\left(\underline{N}(\underline{\theta})^{-1} \frac{d\underline{N}(\underline{\theta})}{d\underline{\theta}} \underline{N}(\underline{\theta})^{-1} \frac{d\underline{N}(\underline{\theta})}{d\underline{\theta}} \right) \right]^{-1}. \tag{9}$$

This computation is performed given the trace function $tr(\cdot)$, anchor-beacon distance matrix $\underline{\theta}$, the gradient of measurement covariance with respect to beacon location $\underline{N}(\underline{\theta})$, and the gradient of measurements with respect to beacon location $\frac{d\underline{m}(\underline{\theta})}{d\underline{\theta}}$ to compute the CRLB of training labels gathered for the fingerprint data. This yielded a standard deviation of 16.8 cm on the x axis and 17.3 cm on the y axis for our ground truth labels.

C. CNN TRAINING

The CNN architecture developed for this work (Fig. 6) was designed using a modified PointNet [51] architecture and a host of over-fitting countermeasures to combat the high noise, low number, and large shift in statistics between training and testing data and labels. The PointNet is terminated with a two neuron linear layer, whose outputs represent the estimated two-dimensional location of the transmitter whose range estimates were input. The model's three-dimensional input represents a set of RSS estimates from the perspective of each sensor for a single detected signal of unknown origin. The PointNet is comprised of two T-nets, each of which is a mini-network comprised of a 32, 64, and 512 filter convolutional layer, a global max pooling [52] layer, a 256 and 128 neuron dense layer, and final dense layer with a number of neurons equal to the squared number of features. We do not change the architecture's depth or width because our inputs are of the same dimensionality as the three-dimensional spatial data that this state-of-the-art architecture was optimized for. These T-nets utilize L2 [53] regularizers ($\lambda = 0.001$) to learn an affine transformation matrix. Each convolutional layer has a kernel size of one, valid zero padding [54], a ReLU (ReLU) activation function, and Kaiming [55] kernel initialization. Additionally, the PointNet is comprised of two sets of convolutional layers with shared weights, a global max pooling layer, and two dense layers with 256 and 128 neurons.

We trained three PointNets in a bagging ensemble [56] learning scheme, which can significantly improve the performance of the trained SL models. A bagging ensemble of SL models is a collection of n models independently trained on the same data set, not to be confused with boosting or stacking ensembles. Bagging ensembles perform regression by averaging their predictions on test data. The benefit of this can be shown by minimizing the expected squared error of predictions, defined as [57]:

$$E\left[\left(\left(\frac{1}{n}\sum_{i=1}^{n}\hat{y}_i\right) - y\right)^2\right] = \frac{v}{n} + c\frac{n-1}{n}, \tag{10}$$

where the variance $v = E[(\hat{y}_i - y_i)^2]$, and the covariance $c = E[(\hat{y}_i - y_j)^2]$, $i \neq j$. If the covariance is zero, or each model makes different mistakes, then the gain of using an ensemble on the squared error of predictions is $\frac{1}{n}$. If $v = c$, then the ensemble brings no gains, and the prediction MSE remains at v.

The weights were optimized in TensorFlow [58] by minimizing training data MSE loss via the Adam [59] quasi-Newton SGD method (Fig. 7). The relatively large difference between the ensemble's loss and each weak learner's loss indicated a low covariance c as described by Eq. (10), or that our use of a bagging ensemble was appropriate and beneficial towards making accurate multilateration estimates. Data was trained in batches of the whole training set, which was of size 601 detected TPMS packets over all 9 locations and 4 transmitters, and batch normalization [60] was used. No early stopping was implemented over the 500 epochs of

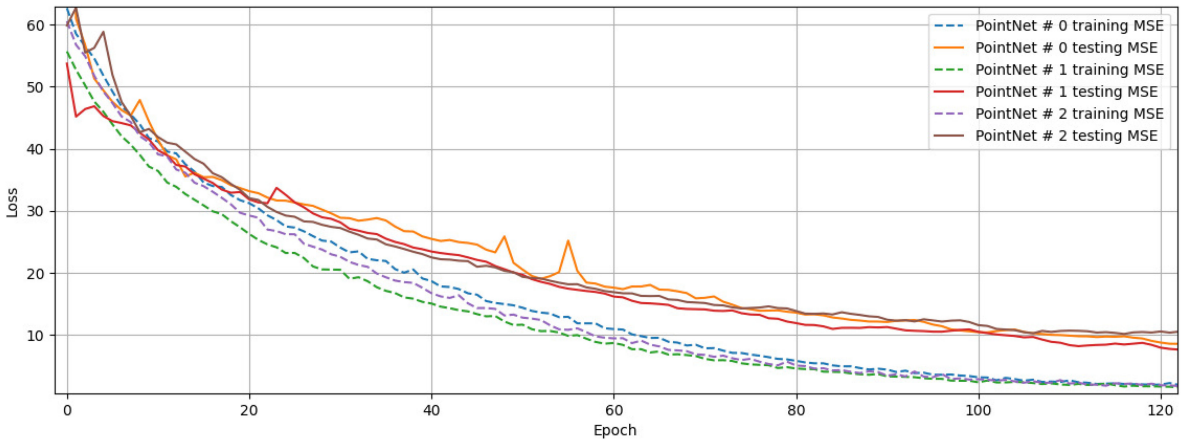

FIGURE 7. The transient epochs of MSE training and validation loss of the CNN. Final training MSE for the ensemble was 0.89 meters, and a final test set MSE of 4.87 meters. CRLB results found that training and test labels have a minimum error of 0.168 m and 0.173 m along the x and y axis, respectively.

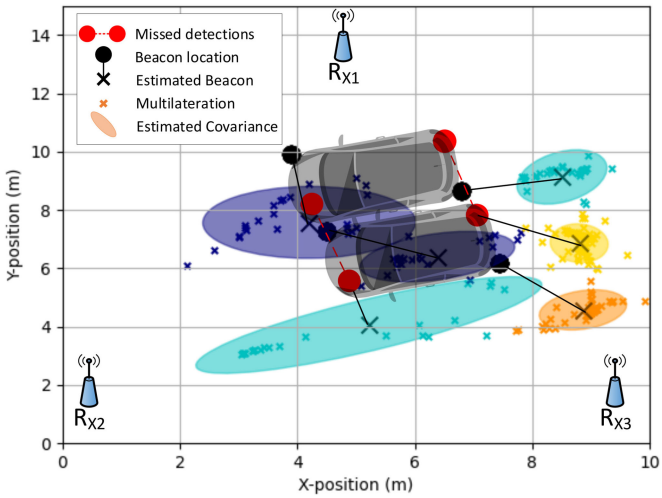

FIGURE 8. A summary of the $N = 229$ spatial multilateration estimates and the estimated cluster means and co-variances of the DPGMM. "Missed detections" represent pairs of transmitters whose spatial and RSS estimates could not be statistically distinguished.

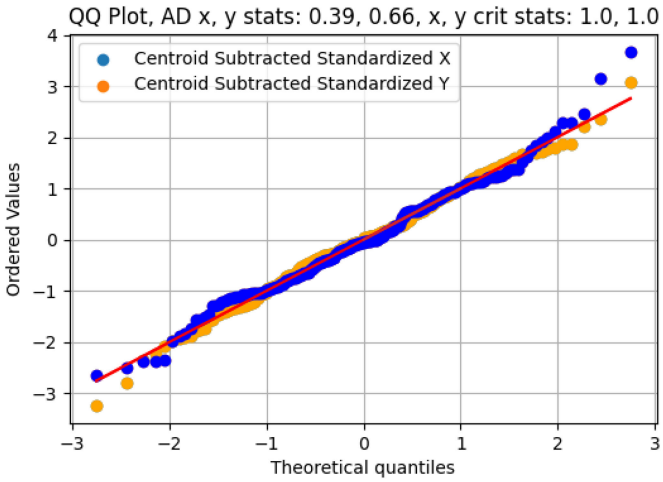

FIGURE 10. QQ plot of the cluster mean subtracted, standardized PointNet multilateration estimates. Additionally, the axis-specific AD statistics and critical statistics are provided.

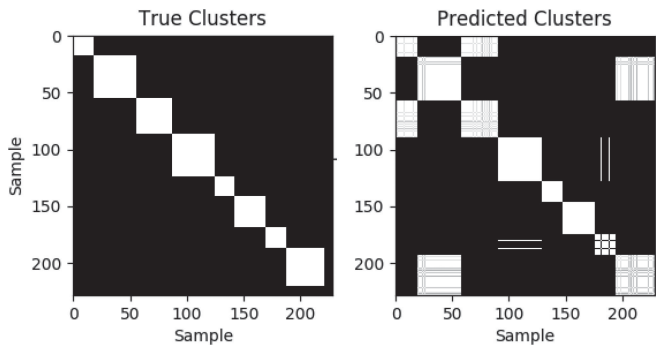

(a) True cluster (b) Predicted cluster

FIGURE 9. A summary of the test set's $N = 229$ detected TPMS packet multilateration estimates true indicator variables $c_i = j, i = 1, \ldots, N$, $j = 1, \ldots, k$ (a) and our predictions (b). Any sample from one axis with the same indicator variable as a sample from the other axis is colored white.

training, at which point the model loss converged. An Intel Core i7-10750H CPU and 16 GB of RAM were sufficient to train this relatively shallow network and low-dimensional data.

D. CNN TESTING & UL INFERENCE

The deployment stage of the proposed SOP beacon localization system used the hardware testbed and algorithms described in this paper. Since physical signal features were estimated, range estimates and subsequently multilateration-based location estimates were random variables [50]. Specifically, location estimates are known to be distributed as multivariate Gaussian variables (even if observations are non-Gaussian [61]–[64]) such that $\hat{P}_i \sim \mathcal{N}(\mu_j, \Sigma_j)$ for a number of multilateration estimates $i = 1, \ldots, N$ and a number of SOP beacons $j = 1, \ldots, k$ [61]–[64]. Consequently, we utilized a DPGMM as a probabilistic inference model with which

to assign the locations estimates $\hat{P}_i$ to k sub-populations. Each sub-population or cluster of estimates represents the spatially-inferred probability that the j^{th} wireless beacon transmitted the i^{th} multilateration estimate (Fig. 3). This inference and assignment method differs from the heuristic methods [17], [19] discussed in Section I since it is automated, leverages the underlying statistics of the data, and is not overly sensitive to hyper-parameter choices.

The evaluation of the experiment can be seen in Fig. 8, in which $N = 229$ detected TPMS packets were localized using the trained CNN. The Autel prompting radio [65] was used for about three minutes at each TPMS beacon location, and the vehicle was moved once for a total of eight beacons, on which we superimposed the multiateration estimates in post-processing. We implemented the DPGMM with $k = N$ such that every data point may become a cluster if its mixing proportion π_j, $j = 1, \ldots, k$ is sufficiently large.

We found the multilateration estimates possessed a high error relative to the distance between beacons. This could potentially be the result of the significant variation in the RSS estimates, the 22.5 dBi directional TPMS antenna [66], or our use of only three receivers, the minimum number required for two-dimensional localization.

The two pairs of RSS populations that could not be differentiated by the EM-based DPGMM clustering were not neighboring locations, but the front-left tire's transmitter and the back-right tire's transmitter at two locations. This indicated a relatively higher correlation between the transmit power and received power than the transmitter location and received power. While only six of the eight RSS populations could be distinguished by the DPGMM, this is actually a typical performance given the small number of sensors, the small size and high variance of the RSS estimates, and the low-power, highly directional design of the transmitters.

We performed a KW (KW) [67] test, a non-normal method for determining if two sets of samples originate from the same distribution. The test statistic is defined as:

$$H = (N-1)\frac{\sum_{i=1}^{g} n_i(\bar{r}_i - \bar{r})^2}{\sum_{i=1}^{g}\sum_{j=1}^{n_i}(r_{ij} - \bar{r})^2}, \tag{11}$$

where N is the number of samples across all groups g, n_i is the number of samples in group i, r denotes rank, and $\bar{\cdot}$ denotes mean. For a critical statistic H^* computed by table lookup for $\alpha = 0.05$, we found $H < H^*$ on the RSS populations of each pair of beacons that made up a missed detection, or that we could not reject the null hypothesis. We could not find evidence the estimates were statistically different. On average, the six beacon estimates were evaluated with ground truth values to have a 1.72 m variance ($E[(\hat{P} - P)^2]$) and 1.19 m bias ($E[|\hat{P} - P|]$).

Insight into the performance of the DPGMM is provided by the confusion matrix which quantifies the accuracy of the expectation step, *i.e.* classification of which transmitter produced which signals (see Fig. 9). The confusion matrix shows the true mixing proportions of the data (Fig. 9(a)) and that some transmitter captures produced more detected signals from the localization sensors than others. That number, from top left to bottom right of the confusion matrix, is [18, 38, 31, 38, 17, 27, 18, 34] detected TPMS packets for each of the three-minute captures at the eight test locations. Alternatively, the confusion matrix also shows that only six of the eight clusters were detected (Fig. 9(b)), as, starting from the top left, if squares are named one through eight, it can be seen the first and third clusters, as well as sixth and eighth clusters are combined. Finally, we can see that two additional multilateration estimates from the seventh beacon are misclassified, producing an indicator variable classification precision or Positive Predictive Value (PPV) of 76.4%. When incorrect cluster assignments caused by missed cluster detections are removed, the PPV is 93.7%. PPV is defined as the number of true positives divided by the sum of true and false positives [68]:

$$\text{PPV} = \frac{\text{TP}}{\text{TP} + \text{FP}}. \tag{12}$$

To gather evidence that our PointNet's location estimates were Gaussian distributed and our use of a Gaussian inference model was suitable, we utilized the AD [69] test for determining if a set of samples are drawn from a particular distribution. To do so, we first subtracted the estimated cluster mean from each population of estimates, then standardized them:

$$Y_i = \frac{(\hat{P}_i - \hat{\mu}_j) - \frac{1}{g}\sum_{i=1}^{g}(\hat{P}_i - \hat{\mu}_j)}{\frac{1}{g-1}\sum_{i=1}^{g}(\hat{P}_i - \frac{1}{g}\sum_{i=1}^{g}(\hat{P}_i - \hat{\mu}_j))^2}. \tag{13}$$

This calculation produced a set of samples that, when tested, whether the estimates were Gaussian with respect to their cluster center. The AD critical value for normal tests can be computed as [70]:

$$A^{*2} = A^2\left(1 + \frac{0.75}{N} + \frac{2.25}{N^2}\right), \tag{14}$$

and the AD statistic is computed as [70]:

$$\begin{aligned} A^2 = &-N - \frac{1}{N}\sum_{i=1}^{N}(2i-1)(\ln \Phi(Y_i) \\ &+ \ln(1 - \Phi(Y_{N+1-i}))), \end{aligned} \tag{15}$$

where Φ is the standard normal CDF (CDF). Our AD results are presented in the QQ (QQ) plot in Fig. 10, which visually and quantitatively show that PointNet multilateration estimates are Gaussian distributed due to the diagonal trend line and small AD test statistics.

V. CONCLUDING REMARKS

In this paper, we demonstrated that a novel self-organizing, stationary transmitter, jointly localizing and classifying methodology could locate transmitters in low meta data scenarios with high accuracy. Hardware experimentation showed that the $N = 229$ spatial test set was able to recognize every statistically different RSS population as verified by a KW test, and was classified with a 76.4% indicator variable PPV (93.7% when accounting for missed cluster detections). The

detected transmitters were localized with an average of 1.71 m variance and 1.19 m bias within a roughly 15 m square whose perimeter is made up of receivers. We confirmed the Gaussian assumption of our clustering algorithm by failing to deny that the PointNet CNN's location predictions were Gaussian distributed. We accomplished this verification via an AD test with critical statistics $A^{*2} = 1.0$ and observed statistics $A^2 = 0.39(0.66)$ for x-axis (y-axis) samples.

Based on the outcomes of this research, several open challenges and opportunities for further research remain.

- The SL-based multilateration architectures could be improved. The current state-of-the-art [28]–[33] uses a denoising auto encoder with unlabelled data and a CNN.
- A different clustering algorithm [71]–[75] than DPGMM may provide better performance depending on the experimental context.
- More robust [21] TDOA datasets could be captured with more expensive hardware than our cost-constrained experiment.

Our methodology allows for the post-multilateration clustering of location estimates such that unknown wireless devices present in driverless vehicles may be opportunistically leveraged for localization tasks, as long as they broadcast detectable emissions from which physical passband characteristics may be estimated from. This lowers reliance on GNSS systems and SOP localization networks that require meta data.

ACKNOWLEDGMENT

The authors would like to thank Allyn Dullighan of MIT Lincoln Laboratory, who provided feedback and directions towards additional works and resources.

DISTRIBUTION STATEMENT

REFERENCES

[1] D. J. Fagnant and K. Kockelman, "Preparing a nation for autonomous vehicles: Opportunities, barriers and policy recommendations," *Transp. Res. Part A: Policy Pract.*, vol. 77, pp. 167–181, 2015.

[2] C. Badue *et al.*, "Self-driving cars: A survey," *Clin. Orthopaedics Related Res.*, 2019. [Online]. Available: http://arxiv.org/abs/1901.04407

[3] C. Rödel, S. Stadler, A. Meschtscherjakov, and M. Tscheligi, "Towards autonomous cars: The effect of autonomy levels on acceptance and user experience," in *Proc. 6th Int. Conf. Automotive User Interfaces Interactive Veh. Appl.*, ser. AutomotiveUI'14. New York, NY, USA: Assoc. Comput. Machinery, 2014, vol. 11, pp 1–11:8. [Online]. Available: http://doi.acm.org/10.1145/2667317.2667330

[4] K. Diepold, K. Götzl, A. Riener, and A. K. Frison, *Automated Driving: Acceptance and Chances for Elderly People*. New York, NY, USA: Assoc. Comput. Machinery, 2017, pp. 163–167.

[5] S. A. Miller and B. R. Heard, "The environmental impact of autonomous vehicles depends on adoption patterns," *Environ. Sci. Technol.*, vol. 50, no. 12, pp. 6119–6121, 2016, doi: 10.1021/acs.est.6b02490.

[6] R. Domínguez, E. Onieva, J. Alonso, J. Villagra, and C. González, "Lidar based perception solution for autonomous vehicles," in *Proc. 11th Int. Conf. Intell. Syst. Des. Appl.*, 2011, pp. 790–795.

[7] J. Janai, F. Güney, A. Behl, and A. Geiger, "Computer vision for autonomous vehicles: Problems, datasets and state-of-the-art," *Clin. Orthopaedics Related Res.*, vol. abs/1704.05519, pp. 195–206, 2017. [Online]. Available: http://arxiv.org/abs/1704.05519

[8] M. Bojarski *et al.*, "End to end learning for self-driving cars," *Clin. Orthopaedics Related Res.*, vol. abs/1604.07316, 2016. [Online]. Available: http://arxiv.org/abs/1604.07316

[9] J. Dickmann *et al.*, "Automotive radar the key technology for autonomous driving: From detection and ranging to environmental understanding," in *Proc. IEEE Radar Conf.*, 2016, pp. 1–6.

[10] W. Rahiman and Z. Zainal, "An overview of development GPS navigation for autonomous car," in *Proc. IEEE 8th Conf. Ind. Electron. Appl.*, 2013, pp. 1112–1118.

[11] M. Zhou, X. Qu, and S. Jin, "On the impact of cooperative autonomous vehicles in improving freeway merging: A modified intelligent driver model-based approach," *IEEE Trans. Intell. Transp. Syst.*, vol. 18, no. 6, pp. 1422–1428, Jun. 2017.

[12] Y. Cui and S. S. Ge, "Autonomous vehicle positioning with GPS in urban canyon environments," *IEEE Trans. Robot. Automat.*, vol. 19, no. 1, pp. 15–25, Feb. 2003.

[13] I.-S. Koh and K. Sarabandi, "Polarimetric channel characterization of foliage for performance assessment of GPS receivers under tree canopies," *IEEE Trans. Antennas Propag.*, vol. 50, no. 5, pp. 713–726, May 2002.

[14] R. L. Fante and J. J. Vaccaro, "Wideband cancellation of interference in a GPS receive array," *IEEE Trans. Aerosp. Electron. Syst.*, vol. 36, no. 2, pp. 549–564, Apr. 2000.

[15] R. H. Mitch *et al.*, "Signal characteristics of civil GPS jammers," in *Proc. 24th Int. Tech. Meeting Satell. Division Inst. Navigat.*, 2011, pp. 1907–1919.

[16] K. A. Fisher, "The navigation potential of signals of opportunity-based time difference of arrival measurements," Ph.D. dissertation, 2005, copyright - Database copyright ProQuest LLC; ProQuest does not claim copyright in the individual underlying works; Accessed: May 25, 2021. [Online]. Available: https://www.proquest.com/dissertations-theses/navigation-potential-signals-opportunity-based/docview/305022658/se-2?accountid=12492

[17] D. Moser, P. Leu, V. Lenders, A. Ranganathan, F. Ricciato, and S. Capkun, "Investigation of multi-device location spoofing attacks on air traffic control and possible countermeasures," in *Proc. 22nd Ann. Int. Conf. Mobile Comput. Netw., ser. MobiCom'16*. New York, NY, USA: Association for Computing Machinery, 2016, pp. 375–386. [Online]. Available: https://doi.org/10.1145/2973750.2973763

[18] M. Schäfer, P. Leu, V. Lenders, and J. Schmitt, "Secure motion verification using the doppler effect," in *Proc. 9th ACM Conf. Secur. Privacy Wireless Mobile Netw.*, 2016, pp. 135–145.

[19] M. Schüfer, V. Lenders, and J. Schmitt, "Secure track verification," in *Proc. IEEE Symp. Secur. Privacy*, 2015, pp. 199–213.

[20] M. Monteiro, A. Barreto, T. Kacem, J. Carvalho, D. Wijesekera, and P. Costa, "Detecting malicious ADS-B broadcasts using wide area multilateration," in *Proc. IEEE/AIAA 34th Digit. Avionics Syst. Conf.*, 2015, pp. 4A3–1.

[21] S. Capkun and J.-P. Hubaux, "Secure positioning of wireless devices with application to sensor networks," in *Proc. IEEE 24th Annu. Joint Conf. IEEE Comput. Commun. Societies*, 2005, vol. 3, pp. 1917–1928.

[22] Y. Chen, W. Trappe, and R. P. Martin, "Attack detection in wireless localization," in *Proc. IEEE INFOCOM 26th IEEE Int. Conf. Comput. Commun.*, 2007, pp. 1964–1972.

[23] J. F., Raquet, and M. Mikel, "Issues and approaches for navigation using signals of opportunity," in *Proc. Nat. Tech. Meeting Inst. Navigation*, 2007, pp. 1073–1080.

[24] J. Morales, P. F. Roysdon, and Z. M. Kassas, "Signals of opportunity aided inertial navigation," in *Proc. 29th Int. Tech. Meeting Satellite Division Inst. Navigation (ION GNSS+ 2016)*, 2016, pp. 1492–1501.

[25] C. Yang, T. Nguyen, and E. Blasch, "Mobile positioning via fusion of mixed signals of opportunity," *IEEE Aerosp. Electron. Syst. Mag.*, vol. 29, no. 4, pp. 34–46, Apr. 2014.

[26] J. A. McEllroy, "Navigation using signals of opportunity in the am transmission band," Air Force Institute of Technology Wright-Patterson Air Force Base Ohio School of Engineering, Tech. Rep. AFIT/GAE/ENG/06-04, 2006.

[27] I. Guvenc and C.-C. Chong, "A survey on TOA based wireless localization and NLOS mitigation techniques," *IEEE Commun. Surv. Tut.*, vol. 11, no. 3, pp. 107–124, Jul.–Sep. 2009.

[28] V. Moghtadaiee, A. G. Dempster, and S. Lim, "Indoor localization using FM radio signals: A fingerprinting approach," in *Proc. Int. Conf. Indoor Positioning Indoor Navigation*, 2011, pp. 1–7.

[29] C. Xiao, D. Yang, Z. Chen, and G. Tan, "3-D BLE indoor localization based on denoising autoencoder," *IEEE Access*, vol. 5, pp. 12 751–12 760, 2017.

[30] X. Zhang, J. Wang, Q. Gao, X. Ma, and H. Wang, "Device-free wireless localization and activity recognition with deep learning," in *Proc. IEEE Int. Conf. Pervasive Comput. Commun. Workshops (PerCom Workshops)*, 2016, pp. 1–5.

[31] M. Mohammadi, A. Al-Fuqaha, M. Guizani, and J. Oh, "Semisupervised deep reinforcement learning in support of IoT and smart city services," *IEEE Internet Things J.*, vol. 5, no. 2, pp. 624–635, Apr. 2018.

[32] M. Ibrahim, M. Torki, and M. Elnainay, "CNN based indoor localization using RSS time-series," in *IEEE Symp. Comput. Commun. (ISCC)*, 2018, pp. 01 044–01 049.

[33] A. Niitsoo, T. Edelhäußer, and C. Mutschler, "Convolutional neural networks for position estimation in TDoA-based locating systems," in *Proc. Int. Conf. Indoor Positioning Indoor Navigation*, 2018, pp. 1–8.

[34] I. N. Sneddon, *Fourier Transforms.* Chelmsford, MA, USA: Courier Corporation, 1995.

[35] P. P. Gandhi and S. A. Kassam, "Optimality of the cell averaging CFAR detector," *IEEE Trans. Inf. Theory*, vol. 40, no. 4, pp. 1226–1228, Jul. 1994.

[36] R. Zhou, Y. Xiong, G. Xing, L. Sun, and J. Ma, "ZIFI: Wireless lan discovery via ZigBee interference signatures," in *Proc. 16th Annu. Int. Conf. Mobile Comput. Netw.*, 2010, pp. 49–60.

[37] A. Norrdine, "An algebraic solution to the multilateration problem," in *Proc. 15th Int. Conf. Indoor Positioning Indoor Navigation*, Sydney, Australia, 2012, vol. 1315.

[38] S. Sonoda and N. Murata, "Neural network with unbounded activation functions is universal approximator," *Appl. Comput. Harmon. Anal.*, vol. 43, no. 2, pp. 233–268, 2017.

[39] J. T. Chiang, J. J. Haas, J. Choi, and Y.-C. Hu, "Secure location verification using simultaneous multilateration," *IEEE Trans. Wireless Commun.*, vol. 11, no. 2, pp. 584–591, Feb. 2012.

[40] C. M. Bishop, *Pattern Recognition and Machine Learning (Information Science and Statistics)*. Berlin, Heidelberg: Springer-Verlag, 2006.

[41] J. Chen, J. Zhu, Y. W. Teh, and T. Zhang, "Stochastic expectation maximization with variance reduction," in *Advances in Neural Information Processing Systems 31*, S. Bengio, H. Wallach, H. Larochelle, K. Grauman, N. Cesa-Bianchi, and R. Garnett, Eds. Red Hook, NY, USA: Curran Associates, Inc., 2018, pp. 7967–7977. [Online]. Available: http://papers.nips.cc/paper/8021-stochastic-expectation-maximization-with-variance-reduction.pdf

[42] M. Kalli, J. Griffin, and S. Walker, "Slice sampling mixture models," *Statist. Comput.*, vol. 21, pp. 93–105, 01 2011.

[43] D. M. Blei and M. I. Jordan, "Variational inference for dirichlet process mixtures," *Bayesian Anal.*, vol. 1, pp. 121–144, 2005.

[44] T. Rydén, "EM versus markov chain monte carlo for estimation of hidden markov models: A computational perspective," *Bayesian Anal.*, vol. 3, no. 4, pp. 659–688, 2008. [Online]. Available: https://projecteuclid.org/euclid.ba/1340370402

[45] S.-h. Jung, B.-c. Moon, and D. Han, "Unsupervised learning for crowdsourced indoor localization in wireless networks," *IEEE Trans. Mobile Comput.*, vol. 15, no. 11, pp. 2892–2906, Nov. 2015.

[46] L. Li, W. Yang, and G. Wang, "HIWL: An unsupervised learning algorithm for indoor wireless localization," in *Proc. 12th IEEE Int. Conf. Trust, Secur. Privacy Computi. Commun.*, 2013, pp. 1747–1753.

[47] Y. Li, X. Hu, Y. Zhuang, Z. Gao, P. Zhang, and N. El-Sheimy, "Deep reinforcement learning (DRL): Another perspective for unsupervised wireless localization," *IEEE Internet Things J.*, vol. 7, no. 7, pp. 6279–6287, Jul. 2020.

[48] L. Li, W. Yang, M. Z. Alam Bhuiyan, and G. Wang, "Unsupervised learning of indoor localization based on received signal strength," *Wireless Commun. Mobile Comput.*, vol. 16, no. 15, pp. 2225–2237, 2016.

[49] K. W. McClintick, M. Page, T. Wickramarathne, and A. M. Wyglinski, "Machine learning-based roadside vehicular traffic localization via opportunistic wireless sensing," in *Proc. IEEE Glob. Conf. Signal Inf. Process.*, 2019, pp. 1–5.

[50] R. Kaune, "Accuracy studies for TDOA and TOA localization," in *Proc. IEEE 15th Int. Conf. Inf. Fusion*, 2012, pp. 408–415.

[51] C. R. Qi, H. Su, K. Mo, and L. J. Guibas, "PointNet: Deep learning on point sets for 3d classification and segmentation," *CoRR*, 2016. [Online]. Available: http://arxiv.org/abs/1612.00593

[52] M. Ranzato, F. J. Huang, Y.-L. Boureau, and Y. LeCun, "Unsupervised learning of invariant feature hierarchies with applications to object recognition," in *Proc. IEEE Conf. Comput. Vis. Pattern Recognit.*, 2007, pp. 1–8.

[53] C. Cortes, M. Mohri, and A. Rostamizadeh, "L2 regularization for learning kernels," in *Proc. 25th Conf. Uncertainty Artif. Intell.*, (ser. UAI'09). Arlington, Virginia, USA: AUAI Press, 2009, pp. 109–116.

[54] S. Albawi, T. A. Mohammed, and S. Al-Zawi, "Understanding of a convolutional neural network," in *Proc. IEEE Int. Conf. Eng. Technol.*, 2017, pp. 1–6.

[55] K. He, X. Zhang, S. Ren, and J. Sun, "Delving deep into rectifiers: Surpassing human-level performance on imagenet classification," in *Proc. IEEE Int. Conf. Comput. Vis.*, 2015, pp. 1026–1034.

[56] D. Opitz and R. Maclin, "Popular ensemble methods: An empirical study," *J. Artif. Intell. Res.*, vol. 11, pp. 169–198, 1999.

[57] M. Sewell, "Ensemble learning," *RN*, vol. 11, no. 02, pp. 1–34, 2008.

[58] M. Abadi *et al.*, "Tensorflow: Large-scale machine learning on heterogeneous distributed systems," in *Proc. 12th USENIX Symp. Operating Syst. Des. Implementation (OSDI 16)*, 2016, pp. 265–283.

[59] D. P. Kingma and J. Ba, "Adam: A method for stochastic optimization," in *Proc. 3rd International Conference on Learning Representations*, San Diego, CA, USA, May 7-9, 2015, Conference Track Proceedings, Y. Bengio and Y. LeCun, Eds., 2015. [Online]. Available: http://arxiv.org/abs/1412.6980

[60] S. Ioffe and C. Szegedy, "Batch normalization: Accelerating deep network training by reducing internal covariate shift," in *Proc. Int. Conf. Mach. Learn.*, 2015, pp. 448–456.

[61] J. Tellinghuisen, "Least squares with non-normal data: Estimating experimental variance functions," *Analyst*, vol. 133, no. 2, pp. 161–166, 2008.

[62] Y. Zhou, J. Li, and L. Lamont, "Multilateration localization in the presence of anchor location uncertainties," in *Proc. IEEE Glob. Commun. Conf.*, 2012, pp. 309–314.

[63] C. Jo and C. Lee, "Multilateration method based on the variance of estimated distance in range-free localisation," *Electron. Lett.*, vol. 52, no. 12, pp. 1078–1080, 2016.

[64] A. Savvides, H. Park, and M.B. Srivastava, "The n-hop multilateration primitive for node localization problems," *Mobile Netw. Appl.*, vol. 8, no. 4, pp. 443–451, 2003.

[65] "TS508 quickstart guide - maxiTPMS," Accessed: Jan. 2021, [Online]. Available: https://www.maxitpms.com/u/cms/www/201804/TS508_Quick%20Guide_V3.pdf

[66] A. Kolodgie *et al.*, "Enhanced TPMS security through acceleration timed transmissions," in *Proc. MILCOM IEEE Mil. Commun. Conf.*, 2017, pp. 35–39.

[67] W. H. Kruskal and W. A. Wallis, "Use of ranks in one-criterion variance analysis," *J. Amer. Stat. Assoc.*, vol. 47, no. 260, pp. 583–621, 1952.

[68] A. Tharwat, "Classification assessment methods," *Appl. Comput. Informat.*, vol. 17, pp. 168–192, 2020.

[69] W. Stefansky, "Rejecting outliers in factorial designs," *Technometrics*, vol. 14, no. 2, pp. 469–479, 1972.

[70] F. W. Scholz and M. A. Stephens, "K-sample anderson-darling tests," *J. Amer. Stat. Assoc.*, vol. 82, no. 399, pp. 918–924, 1987.

[71] B. J. Frey and D. Dueck, "Clustering by passing messages between data points," *Science*, vol. 315, no. 5814, pp. 972–976, 2007.

[72] D. Comaniciu and P. Meer, "Mean shift: A robust approach toward feature space analysis," *IEEE Trans. Pattern Anal. Mach. Intell.*, vol. 24, no. 5, pp. 603–619, May 2002.
[73] M. Ester *et al.*, "A density-based algorithm for discovering clusters in large spatial databases with noise." *KDD*, vol. 96, no. 34, 1996, pp. 226–231.
[74] M. Ankerst, M. M. Breunig, H.-P. Kriegel, and J. Sander, "Optics: Ordering points to identify the clustering structure," *ACM SIGMOD Rec.*, vol. 28, no. 2, pp. 49–60, 1999.
[75] T. Zhang, R. Ramakrishnan, and M. Livny, "BIRCH: An efficient data clustering method for very large databases," *ACM SIGMOD Rec.*, vol. 25, no. 2, pp. 103–114, 1996.

KYLE W. MCCLINTICK (Student Member, IEEE) received the B.S. degree in electrical and computer engineering from the Rose-Hulman Institute of Technology, Terre Haute, IN, USA, in 2017, and the M.S. degree in electrical and computer engineering from Worcester Polytechnic Institute, Worcester, MA, USA, in 2019, with a thesis on supervised learning in wireless communications, generously funded by The MITRE Corporation. He is currently working toward the Ph.D. degree with the Department of Electrical and Computer Engineering, with a data science and computer science minor, generously funded by MIT Lincoln Laboratory. He was awarded the Best Paper Award for his GlobalSIP 2019 paper, and was awarded the 2019 SMART Ph.D. fellowship, sponsored by NAWCWD Point Mugu, CA, USA.

JEFFREY TOLBERT (Student Member, IEEE) received the B.S. degree in electrical and computer engineering and the B.S. degree in robotics engineering in 2018 from Worcester Polytechnic Institute, Worcester, MA, USA, where he is currently working toward the master's degree, with a focus on wireless communications and digital signal processing. He is also a full time Communication Systems Engineer with The MITRE Corporation.

ALEXANDER M. WYGLINSKI (Senior Member, IEEE) received the B.Eng. degree in electrical engineering from McGill University, QC, Montreal, Canada, in 1999, the M.Sc.(Eng.) degree in electrical engineering from Queen's University, Kingston, ON, Canada, in 2000, and the Ph.D. degree in electrical engineering from McGill University, in 2005. He is currently the Associate Dean of Graduate Studies and a Professor of electrical and computer engineering with Worcester Polytechnic Institute (WPI), Worcester, MA, USA, and also the Director of the Wireless Innovation Laboratory with WPI. He has authored or coauthored more than 48 peer-reviewed journal papers, more than 125 peer-reviewed conference papers, and three textbooks throughout his academic career. His research interests include wireless communications, cognitive radio, machine learning for wireless systems, software defined radio prototyping, connected and autonomous vehicles, and dynamic spectrum sensing. Dr. Wyglinski was the President of the IEEE Vehicular Technology Society during 2018–2019. He was sponsored by both goverment agencies and industry, such as the National Science Foundation, Office of Naval Research, Air Force Research Laboratory, MIT Lincoln Laboratory, Toyota InfoTechnology Center USA, Verizon, MITRE, Analog Devices, and Raytheon.